PNAS RESEARCH ARTICLE | NEUROSCIENCE

Autophagy protein ULK1 interacts with and regulates SARM1 during axonal injury

Harry M. C. Choi[a], Yun Li[a], Delwin Suraj[a], Ru-Ching Hsia[b,1], Chinmoy Sarkar[a], Junfang Wu[a,2], and Marta M. Lipinski[a,2]

Edited by Ana Maria Cuervo, Albert Einstein College of Medicine, Bronx, NY; received March 3, 2022; accepted September 17, 2022

Autophagy is a cellular catabolic pathway generally thought to be neuroprotective. However, autophagy and in particular its upstream regulator, the ULK1 kinase, can also promote axonal degeneration. We examined the role and the mechanisms of autophagy in axonal degeneration using a mouse model of contusive spinal cord injury (SCI). Consistent with activation of autophagy during axonal degeneration following SCI, autophagosome marker LC3, ULK1 kinase, and ULK1 target, phospho-ATG13, accumulated in the axonal bulbs and injured axons. SARM1, a TIR NADase with a pivotal role in axonal degeneration, colocalized with ULK1 within 1 h after SCI, suggesting possible interaction between autophagy and SARM1-mediated axonal degeneration. In our in vitro experiments, inhibition of autophagy, including *Ulk1* knockdown and ULK1 inhibitor, attenuated neurite fragmentation and reduced accumulation of SARM1 puncta in neurites of primary cortical neurons subjected to glutamate excitotoxicity. Immunoprecipitation data demonstrated that ULK1 physically interacted with SARM1 in vitro and in vivo and that SAM domains of SARM1 were necessary for ULK1–SARM1 complex formation. Consistent with a role in regulation of axonal degeneration, in primary cortical neurons ULK1–SARM1 interaction increased upon neurite damage. Supporting a role for autophagy and ULK1 in regulation of SARM1 in axonal degeneration in vivo, axonal ULK1 activation and accumulation of SARM1 were both decreased after SCI in *Becn1*$^{+/-}$ autophagy hypomorph mice compared to wild-type (WT) controls. These findings suggest a regulatory crosstalk between autophagy and axonal degeneration pathways, which is mediated through ULK1–SARM1 interaction and contributes to the ability of SARM1 to accumulate in injured axons.

autophagy | spinal cord injury | mouse models | axonal degeneration

Axonal degeneration contributes to irreversible neuronal dysfunction in neurodegenerative diseases and neurotrauma, but the underlying mechanisms are not fully understood. Recent data demonstrate that the sterile alpha and TIR motif containing 1 (SARM1), the TIR NAD^+ nucleotidase (NADase) (1–3), translocates to injured axons and plays an indispensable role in the mediation of acute axonal degeneration (4–6). Consistently, knocking out *Sarm1* in mouse models of axonal injury attenuated structural and behavioral deficits (7, 8). However, how SARM1 is regulated in the context of axonal degeneration is not fully understood.

In addition to SARM1, recent data implicate a role for macroautophagy (hereafter autophagy) in the mediation of axonal degeneration. Autophagy is a lysosome-dependent catabolic pathway important for cellular homeostasis. Initiation of autophagy requires interaction between the unc-51 like autophagy activating kinase 1 (ULK1) protein kinase and the class III PI3K complex including BECN1 (9). Generally, autophagy is considered to be neuroprotective, and its inhibition is implicated in both neurodegenerative diseases and neurotrauma. However, studies specifically examining acute axonal degeneration indicate that autophagy and particularly ULK1 activity is involved in the mediation of axonal injury. Wakatsuki et al. (10) demonstrated that inhibition of autophagy could delay axonal degeneration in vitro and suggested that autophagy might provide local adenosine 5′-triphosphate/energy for the active axonal degeneration process. In vivo inhibition of autophagy could attenuate axonal degeneration in optic nerve crush (11) and spinal cord injury (SCI) models (12). Furthermore, Vahsen et al. (12) elegantly demonstrated specific involvement of ULK1 in axonal degeneration in vitro and in vivo through its influence on mammalian target of rapamycin (mTOR) activity, translation, and splicing. However, it remains unknown whether and how autophagy may interact with the SARM1-dependent axonal degeneration pathway.

In the current study, we demonstrate that autophagy markers including activated ULK1 colocalize with SARM1 in injured axons in vivo after SCI in mice. Inhibition of ULK1 in primary cortical neurons attenuated SARM1 accumulation in the neurites and

Significance

Axonal degeneration is observed and plays an important role in acute central nervous system injury and in neurodegenerative diseases. Previous studies found that autophagy, a cellular catabolic pathway generally thought to be neuroprotective, can promote axonal degeneration through a mechanism that remains poorly understood. Our studies of axonal degeneration in a mouse model of spinal cord injury (SCI) demonstrate a functional and physical interaction between upstream regulator of autophagy ULK1 and the essential axonal degeneration mediator SARM1. Our findings suggest a direct regulatory crosstalk between autophagy and axonal degeneration pathways, which is mediated through ULK1–SARM1 interaction and contributes to the ability of SARM1 to accumulate in injured axons.

Author affiliations: [a]Shock, Trauma and Anesthesiology Research Center, Department of Anesthesiology, University of Maryland School of Medicine, Baltimore, MD 21201; and [b]Electron Microscopy Core Imaging Facility, Center for Innovative Biomedical Resources, University of Maryland Baltimore, Baltimore, MD 21201

Author contributions: H.M.C.C., R.-C.H., C.S., J.W., and M.M.L. designed research; H.M.C.C., Y.L., D.S., R.-C.H., and C.S. performed research; H.M.C.C., R.-C.H., and M.M.L. analyzed data; H.M.C.C., and M.M.L. wrote the paper; and J.W. and M.M.L. provided funding.

The authors declare no competing interest.

This article is a PNAS Direct Submission.

[1]Present address: Department of Embryology, Carnegie Institution for Science, Baltimore, MD 21218.

[2]To whom correspondence may be addressed. Email: junfang.wu@som.umaryland.edu or mlipinski@som.umaryland.edu.

This article contains supporting information online at http://www.pnas.org/lookup/suppl/doi:10.1073/pnas.2203824119/-/DCSupplemental.

Published November 14, 2022.

neurite degeneration. ULK1 and SARM1 physically interacted in HEK293T cells, primary neurons and mouse spinal cord, and the ULK1–SARM1 interaction was enhanced following neurite injury in primary neurons. SCI in autophagy hypomorph *Becn1*$^{+/-}$ mice led to decreased activation of ULK1 and attenuated accumulation of SARM1 in the injured axons. These findings implicate autophagy and ULK1–SARM1 interaction in the regulation of SARM1 axonal localization after injury and its ability to promote axonal degeneration.

Results

Autophagosomes Accumulate in Axons and Axonal Bulbs after SCI. To explore the involvement of autophagy in axonal damage after SCI, we inflicted moderate contusive SCI at the T10 level in *GFP-LC3* transgenic autophagy reporter mice (13). Under autophagy-promoting conditions, LC3 protein is lipidated and translocates to autophagosomes; an increase in intracellular green fluorescent protein (GFP)-LC3 puncta reflects accumulation of autophagosomes (14). One day after SCI, the GFP-LC3 signal increased dramatically in the white matter of the spinal cord and especially in spherical bulb-like structures around the injury site (Fig. 1*A*). To investigate the spatiotemporal characteristics of the LC3$^+$ bulb structures, we quantified their abundance and size over time from 1 h to 7 d (168 h) after injury (Fig. 1 *B* and *C* and *SI Appendix*, Fig. S1 *A* and *B*). The LC3$^+$ bulb structures started to accumulate by 6 h and peaked in both number and size at 1 d after injury. They were most abundant in the dorsal column rostral to the injury (RD area; Fig. 1*B* and *SI Appendix*, Fig. S1).

The dorsal column of the spinal cord includes both ascending and descending tracts. The ascending tract, fasciculus gracilis (Gr), would be expected to have proximal stumps of axons from the dorsal root ganglion caudal and distal stumps rostral to the injury site. Conversely, the descending corticospinal tract (CST) would be expected to have proximal stumps from the cortical neurons rostral and distal stumps caudal to the injury (*SI Appendix*, Fig. S2*A*). To determine whether LC3$^+$ bulbs may preferentially form at the distal or proximal stumps of the severed axons, we stained sections with antibodies against PKCγ, which is expressed in CST but not Gr neurons. For both tracts, the density of the LC3$^+$ bulb structures was significantly higher in the area rostral to the injury, which includes proximal stumps of CST but distal stumps of Gr (*SI Appendix*, Fig. S2*B*). This suggests that bulb formation is affected more by the location in respect to the injury site (rostral) rather than by the direction of the axonal tract.

Apart from the larger bulb structures (up to 40 μm in diameter), the GFP-LC3 signal was also found to accumulate in TUBB3$^+$ injured axons (typically <5 μm in diameter) in the dorsal column after SCI (Fig. 1 *C* and *D* and *SI Appendix*, Fig. S3*A*). Accumulation of autophagy markers has been reported in injured axons and axonal bulbs at severed axonal endings in rat optic nerve crush and SCI models (11, 12, 15). To confirm that the LC3$^+$ bulb structures in SCI mice correspond to axonal bulbs, we examined their colocalization with different cellular markers. The LC3$^+$ bulb structures did not colocalize with DAPI or the glial fibrillary acidic protein (GFAP), indicating that they were not cell bodies or astrocytes (*SI Appendix*, Fig. S3 *B*, *C*, and *E*). There was also little overlap between LC3 staining on sections from mice expressing microglial marker CX3CR1-GFP (*SI Appendix*, Fig. S3 *D* and *E*). Colocalization between LC3 and the neurite injury marker SMI32 confirmed that LC3$^+$ bulb structures are swollen axonal bulbs at the stumps of damaged axons (Fig. 1 *E* and *F* and *SI Appendix*, Fig. S3*E*).

We used correlative light/electron microscopy (EM) to visualize the ultrastructure of the LC3$^+$ axonal bulbs. Using the surrounding nuclei as reference (*SI Appendix*, Fig. S4*A*), we aligned fluorescent GFP-LC3$^+$ bulb images with EM images (*SI Appendix*, Fig. S4*B*). The representative LC3$^+$ bulb had an axonal ultrastructure of cytoplasm surrounded by myelin but was very swollen compared to the intact axons in the dorsal white matter of a naive mouse (Fig. 1*G*) and was filled with multilamellar autophagic vacuoles containing mitochondria and ribosomes (Fig. 1*H*). Additionally, electron-dense lysosomes/autolysosomes were clearly apparent. These data confirm that the LC3$^+$ bulb structures in the white matter of injured spinal cord are axonal bulbs filled with accumulating autophagic vacuoles.

ULK1 Is Activated and Colocalizes with SARM1 in Axons and Axonal Bulbs after SCI. To determine whether autophagy may be activated in injured axons, we examined the expression of autophagy mediators in the RD white matter after injury. Consistent with the EM data showing cargo-containing autophagic vacuoles accumulating in the axonal bulbs (Fig. 1 *G* and *H*), many LC3$^+$ axonal bulbs colocalized with the autophagy cargo adaptor protein p62/SQSTM (Fig. 2 *A* and *B* and *SI Appendix*, Fig. S5*A*). Both the regulator of autophagy initiation ULK1 and its phosphorylation target ATG13 p-S318 (16) also accumulated in LC3$^+$ axonal bulbs with a peak between 6 and 24 h after injury and colocalized with each other (Fig. 2 *C*–*H* and *SI Appendix*, Fig. S5 *B*–*D*). The colocalization suggests that ULK1 is likely responsible for ATG13 phosphorylation and autophagy initiation in the axonal bulbs. In addition to the swollen axonal bulbs, we also observed colocalization of GFP-LC3 and ULK1 in injured but nonswollen axons after SCI. Interestingly, in the injured axons ULK1 accumulated at a much earlier time point, with a peak between 1 and 6 h after injury (Fig. 2 *I* and *J* and *SI Appendix*, Fig. S5*E*).

To investigate the interaction between autophagy and axonal degeneration pathways, we examined localization of SARM1, a key mediator of axonal degeneration (2, 17–19) in injured axons and axonal bulbs. SARM1 colocalized to the LC3$^+$ and ULK1$^+$ axonal bulbs with a peak between 6 and 24 h after injury (Fig. 3 *A*–*D* and *SI Appendix*, Fig. S5 *F* and *G*). Several other molecules involved in axonal degeneration and implicated in the SARM1 pathway, including MAP3K12 (2, 18, 20–24) and MYCBP2 (24–26), also colocalized to LC3$^+$ and ULK1$^+$ axonal bulbs (*SI Appendix*, Fig. S6). SARM1 also accumulated in injured but nonswollen axons. In axons, SARM1 expression peaked at 1 d after SCI (Fig. 3 *E* and *F* and *SI Appendix*, Fig. S5*H*). Interestingly, colocalization between ULK1 and SARM1 in axons started within 1 h after injury (Fig. 3 *G* and *H* and *SI Appendix*, Fig. S5*I*), suggesting the possibility that interaction between the two pathways may represent an apical event in axonal degeneration after SCI. These findings demonstrate that autophagy and axonal degeneration pathways are activated in the injured axons and axonal bulbs and suggest the possibility that autophagy may interact with the SARM1-mediated axonal injury and degeneration pathway.

Inhibition of Autophagy Attenuates Neurite Degeneration and SARM1 Accumulation in Neurites. Glutamate excitotoxicity is one of the mechanisms contributing to neuronal injury after SCI (27). To further investigate the interaction between autophagy and axonal degeneration pathways, we treated mouse primary cortical neurons with glutamate as a model of SCI-relevant axonal

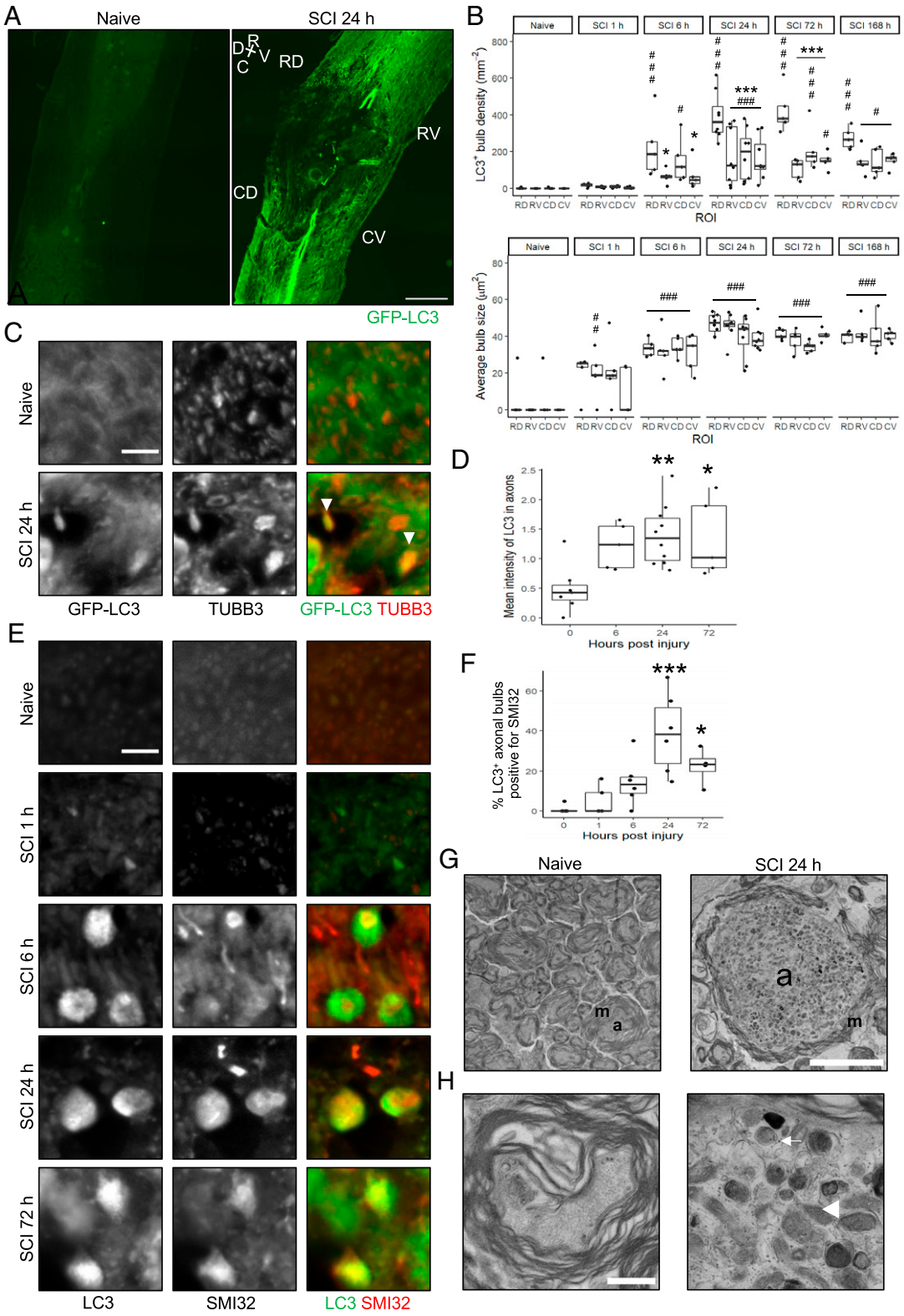

Fig. 1. Autophagosomes accumulate in the injured axons and axonal bulbs after SCI. (*A*) Accumulation of GFP-LC3 (green) 24 h after a thoracic T10 contusion SCI in the spinal cord of *GFP-LC3* transgenic autophagy reporter mice. Sagittal sections across the injury site are shown; R, rostral; C, caudal; D, dorsal; V, ventral; RD, rostro-dorsal; RV, rostro-ventral; CD, caudo-dorsal; CV, caudo-ventral. Scale bar, 500 μm. (*B*) Quantification of data from *A* and *SI Appendix*, Fig. S1 *A* and *B* (magnified images of RD, RV, CD, and CV areas over time). The number, density, and size of $LC3^+$ bulbs peaked at 24 h after SCI preferentially in the RD area. #$P < 0.05$, ##$P < 0.01$, ###$P < 0.001$ versus naive for the same area (RD, RV, CD, CV); *$P < 0.05$, ***$P < 0.001$ versus RD at the same time point after SCI (two-way ANOVA, $n = 5$ to 8). (*C* and *D*) Coronal sections from *GFP-LC3* mice 24 h after SCI demonstrating accumulation of GFP-LC3 in $TUBB3^+$ injured but nonswollen axons (arrowheads) in the RD area of the spinal cord. Scale bar, 10 μm; *$P < 0.05$, **$P < 0.01$ versus naive (one-way ANOVA, $n = 5$ to 10). (*E* and *F*) Time course of GFP-LC3 accumulation in swollen axonal bulbs marked with SMI32 in the RD area after SCI. Scale bar, 30 μm; *$P < 0.05$, ***$P < 0.001$ versus naive (one-way ANOVA, $n = 4$ to 6). (*G*) EM images comparing normal axons in naive mice and axons in the RD area swollen to form axonal bulbs 24 h after SCI. Scale bar, 5 μm. a, axon; m, myelin. (*H*) Higher resolution images from the same area as in *G* showing one naive axon without obvious autophagic vacuoles (*Left*) and accumulated autophagic vacuoles containing mitochondria (arrowhead) and ribosomes (arrow) present in an axonal bulb 24 h after SCI (*Right*). Scale bar, 0.5 μm. Each data point represents an individual mouse; boxplots show median and IQR measures.

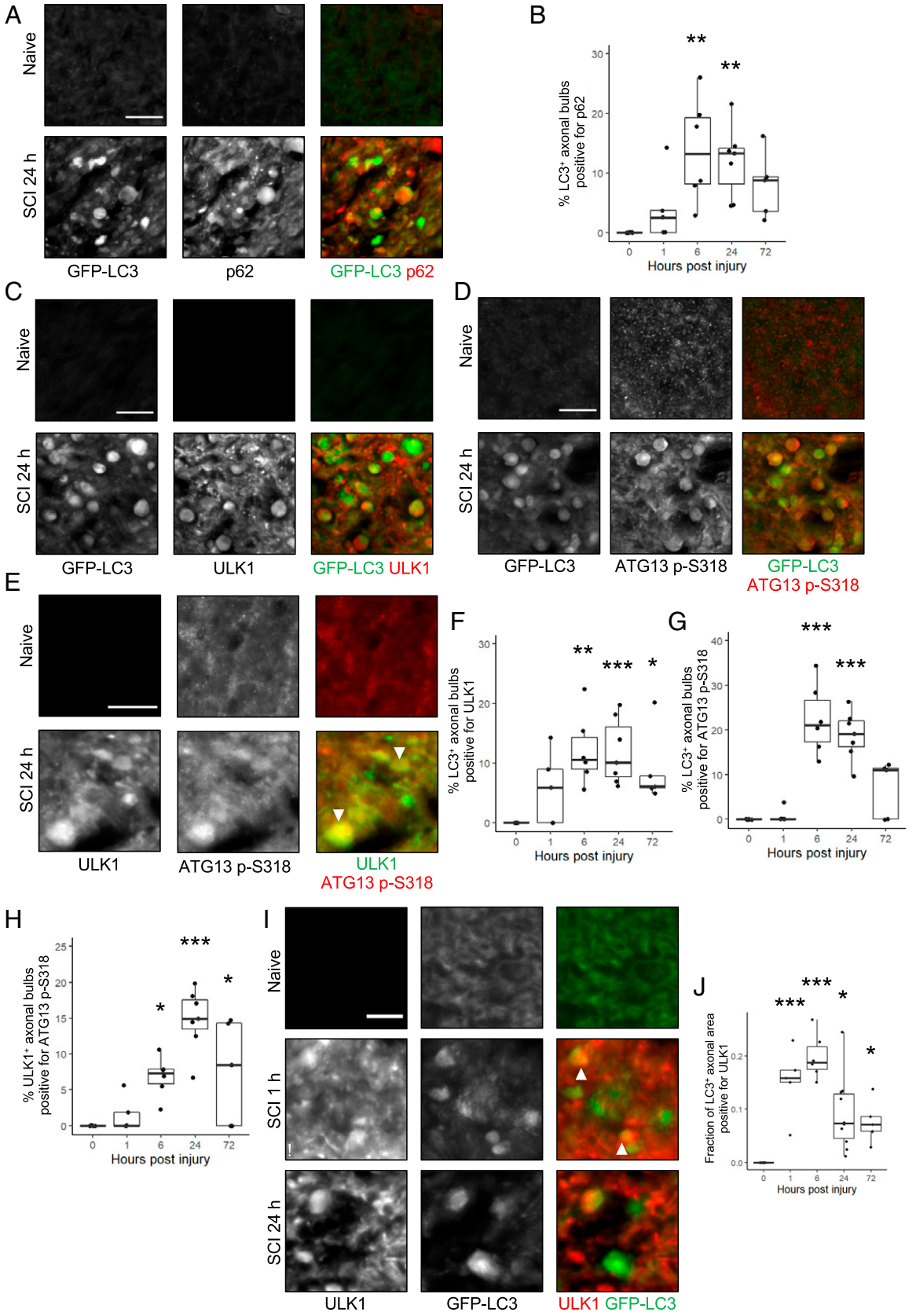

Fig. 2. ULK1 is activated in injured axons and axonal bulbs after SCI. (*A* and *B*) Colocalization between GFP-LC3 and p62 in swollen axonal bulbs in the RD area of the spinal cord 24 h after SCI. Scale bar, 30 μm; $^{**}P < 0.01$ versus naive (one-way ANOVA, $n = 5$ to 7). (*C* and *D*) Accumulation of ULK1 and its target phospho-S318 ATG13 in GFP-LC3^{+} axonal bulbs at 24 h after SCI. Scale bar, 30 μm. (*E*) Colocalization of ULK1 and ATG13 phospho-S318 in axonal bulbs (arrowheads) at 24 h after SCI. Scale bar, 20 μm. (*F–H*) Quantification of colocalization data from *C–E*. $^{*}P < 0.05$, $^{**}P < 0.01$, $^{***}P < 0.001$ versus naive (one-way ANOVA, $n = 5$ to 7). (*I* and *J*) Time course of colocalization between ULK1 and GFP-LC3 in injured but nonswollen axons (arrowheads) after SCI. Scale bar, 10 μm. Brightness and contrast of the image marked with ! were decreased to allow better visualization of all channels in the overlay image. $^{*}P < 0.05$, $^{***}P < 0.001$ versus naive (one-way ANOVA, $n = 5$ to 9). Each data point represents an individual mouse; boxplots show median and IQR measures.

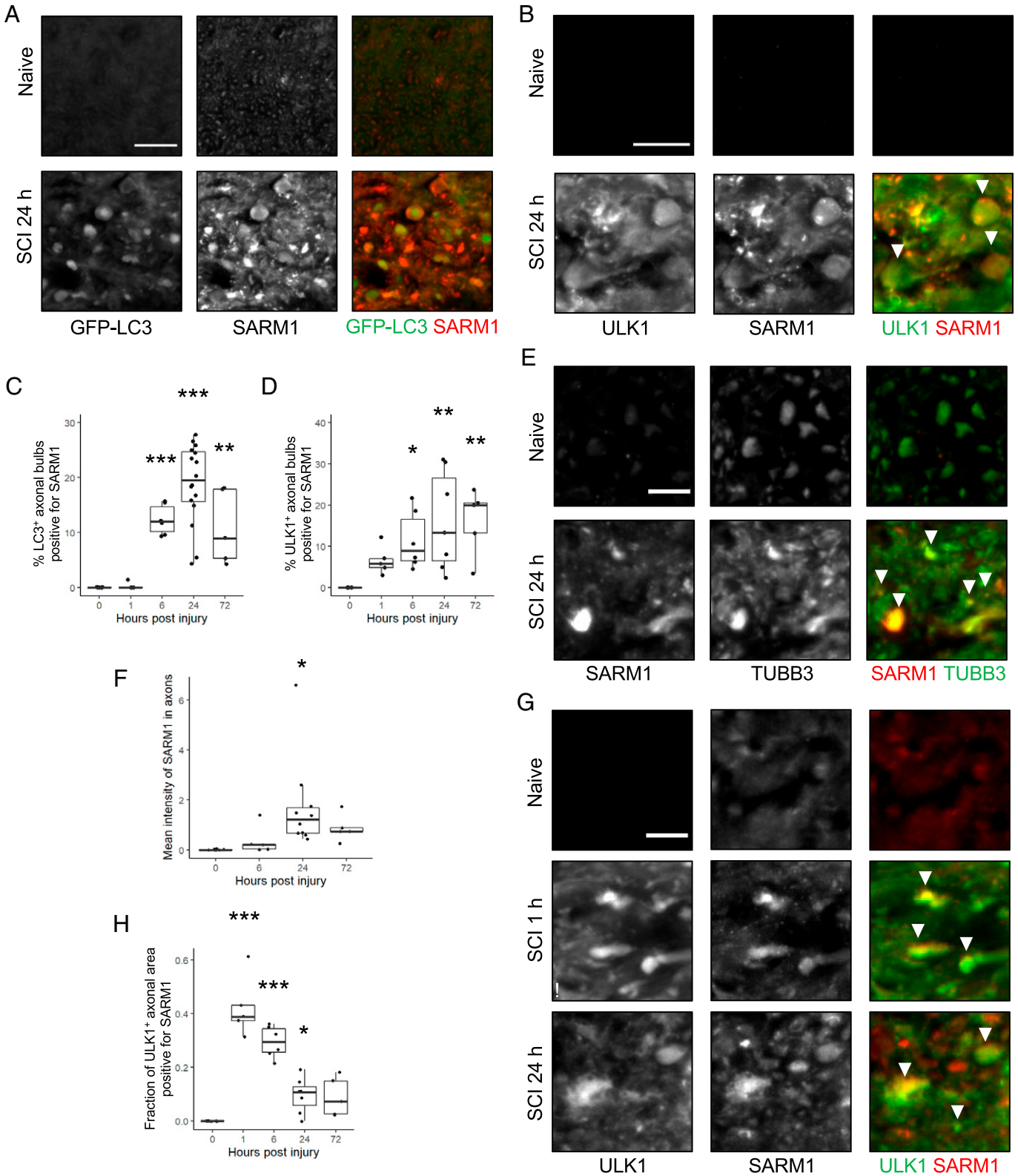

Fig. 3. ULK1 and SARM1 colocalize in injured axons and axonal bulbs after SCI. (*A* and *B*) Colocalization of autophagy markers GFP-LC3 and ULK1 with SARM1 in swollen axonal bulbs in the RD area of the spinal cord 24 h after SCI. Scale bars, 30 μm (*A*), 20 μm (*B*). (*C* and *D*) Quantification of colocalization data from *A* and *B*. **P* < 0.05, ***P* < 0.01, ****P* < 0.001 versus naive (one-way ANOVA, *n* = 5 to 16). (*E* and *F*) Accumulation of SARM1 in injured but nonswollen TUBB3⁺ axons (arrowheads) 24 h after SCI. Scale bar, 10 μm. **P* < 0.05 versus naive (one-way ANOVA, *n* = 5 to 10). (*G* and *H*) Time course of colocalization between ULK1 and SARM1 in injured axons (arrowheads) after SCI. Scale bar, 10 μm. Brightness and contrast of the image marked with ! were decreased to allow better visualization of all channels in the overlay images. **P* < 0.05, ****P* < 0.001 versus naive (one-way ANOVA, *n* = 5 to 7). Each data point represents an individual mouse; boxplots show median and IQR measures.

injury (28). Glutamate caused significant neurite fragmentation starting at 1 h and continuing at 2- and 4-h time points (Fig. 4 *A* and *B*) but did not affect autophagy flux (*SI Appendix*, Fig. S7 *A* and *B*). Treatment with 3-methyladenine (3MA), which inhibits class III PI3K essential for autophagy initiation (*SI Appendix*, Fig. S7*C*), chloroquine (CHQ), which neutralizes lysosomal pH

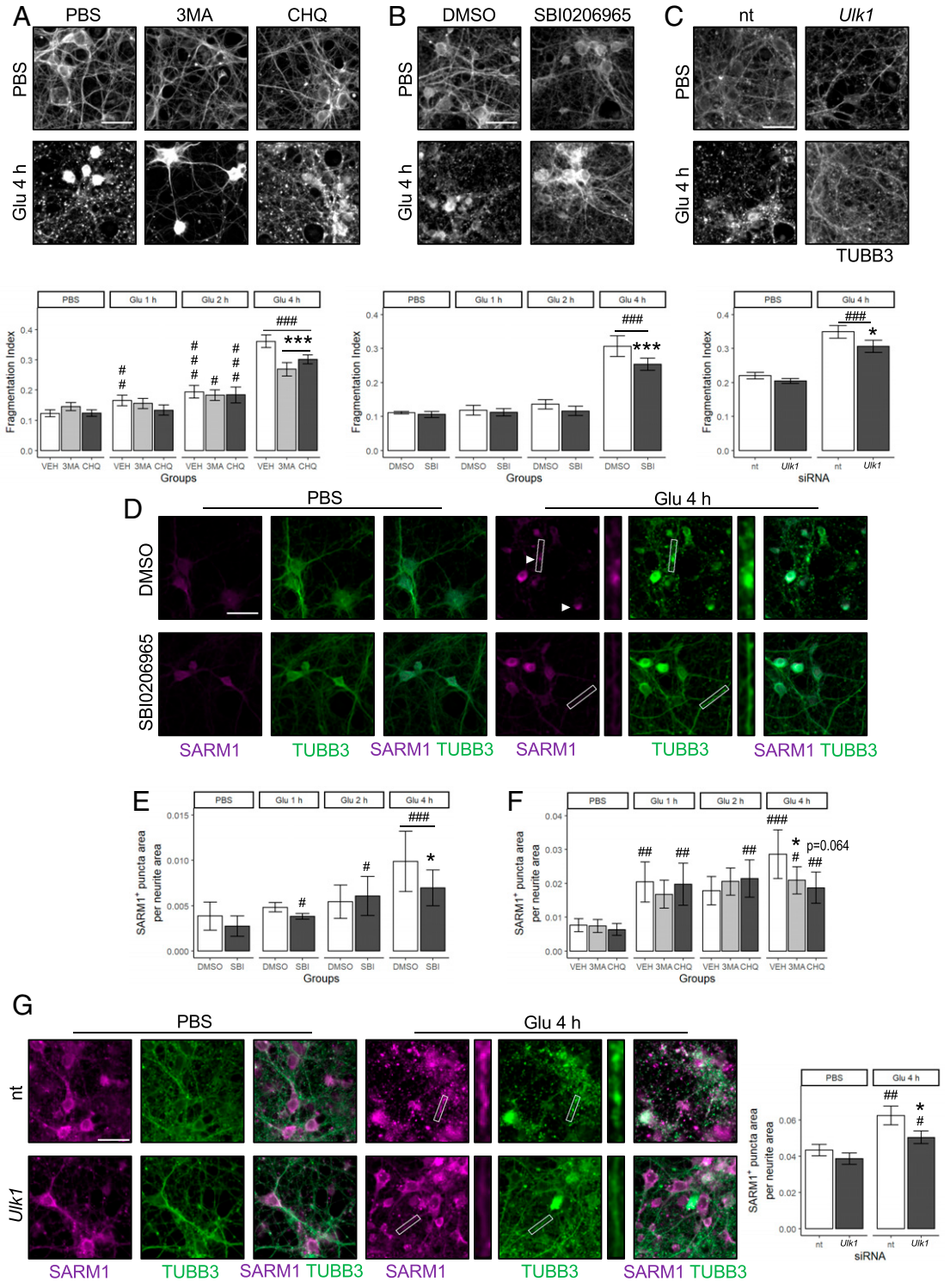

Fig. 4. Inhibition of autophagy and ULK1 activity attenuates neurite fragmentation and SARM1 accumulation in neurites in vitro. (*A*) Primary mouse cortical neurons were treated with glutamate (Glu; 12.5 μM) in the presence of vehicle (phosphate-buffered saline [PBS]), 3MA (10 mM), or CHQ (100 μM). Neurite fragmentation was visualized by TUBB3 staining. Both 3MA and CHQ significantly attenuated glutamate-induced neurite fragmentation at 4 h. Scale bar, 30 μm. #$P < 0.05$, ##$P < 0.01$, ###$P < 0.001$ versus no glutamate (PBS) controls treated with the same drugs (PBS, 3MA, or CHQ); ***$P < 0.001$ versus PBS vehicle (veh) at the same time point (two-way ANOVA). (*B*) Neurons were treated with glutamate in the presence of vehicle (dimethyl sulfoxide [DMSO]) or ULK1 inhibitor SBI (10 μM). SBI significantly attenuated glutamate-induced neurite fragmentation at 4 h. Scale bar, 30 μm; ###$P < 0.001$ versus no glutamate (PBS) controls treated with the same drugs (DMSO or SBI); ***$P < 0.001$ versus vehicle (DMSO) at the same time point (two-way ANOVA). (*C*) Neurons pretreated with either nt siRNA or siRNA against *Ulk1* were treated with glutamate. *Ulk1* knockdown significantly reduced neurite fragmentation at 4 h. Scale bar, 30 μm. ###$P < 0.001$ versus no glutamate (PBS) controls with same siRNA (nt or *Ulk1*); *$P < 0.05$ versus nt siRNA at the same time point (two-way ANOVA). (*D–F*) Glutamate treatment led to accumulation of SARM1 in neuronal cell bodies and of SARM1 puncta in neurites (arrowheads and insets). Treatment with ULK1 inhibitor SBI (*D* and *E*) or autophagy inhibitors 3MA and CHQ (*F*; data shown in *SI Appendix*, Fig. S8*A*) attenuated SARM1 puncta accumulation in neurites but not in cell bodies. Scale bar, 30 μm. #$P < 0.05$, ##$P < 0.01$, ###$P < 0.001$ versus no glutamate (PBS) treated with the same drug (PBS, 3MA, CHQ, DMSO, or SBI); *$P < 0.05$ versus vehicle (PBS or DMSO) at the same time point (two-way ANOVA). (*G*) siRNA-mediated *Ulk1* knockdown significantly reduced SARM1 puncta accumulation in neurites after 4-h glutamate treatment. Scale bar, 30 μm. #$P < 0.05$, ##$P < 0.01$ versus no glutamate (PBS) controls with the same siRNA (nt or *Ulk1*); *$P < 0.05$ versus nt siRNA at the same time point (two-way ANOVA). At least $n = 3$ independent preparations of mouse cortical neurons were used for each experiment. Data are presented as mean ± SEM.

and prevents autophagosome-lysosome fusion, or SBI0206965 (SBI), an ULK1 kinase inhibitor (*SI Appendix*, Fig. S7*D*), attenuated glutamate-induced neurite fragmentation (Fig. 4 *A* and *B* and *SI Appendix*, Fig. S8*A*). To further examine the role of autophagy in neurite degeneration using genetic rather than pharmacological manipulation, we treated neurons with control nontargeting (nt) small interfering RNA (siRNA) or siRNA against *Ulk1*. siRNA-mediated knockdown of *Ulk1* (*SI Appendix*, Fig. S8*B*) was able to significantly reduce neurite fragmentation 4 h after glutamate treatment (Fig. 4*C*).

To investigate the effects of inhibition of autophagy on SARM1, we performed SARM1 immunostaining in cortical neurons treated with glutamate and 3MA, CHQ, or SBI. Following glutamate treatment, SARM1 levels increased in both cell bodies and neurites (Fig. 4 *D*–*F* and *SI Appendix*, Fig. S8*A*). In the neurites, SARM1 accumulated in distinct puncta. Autophagy inhibition by 3MA, CHQ, or SBI decreased accumulation of SARM1 in the neurites but not in the neuronal cell bodies (Fig. 4 *D*–*F* and *SI Appendix*, Fig. S8*A*). Similarly, siRNA-mediated knockdown of *Ulk1* was able to attenuate formation of SARM1 puncta in neurites after glutamate treatment (Fig. 4*G*). These data suggest that autophagy, and particularly ULK1, may affect neurite degeneration by regulating SARM1 accumulation in the injured neurites.

Some of the autophagy proteins, including ULK1, are known to have additional autophagy-independent functions (29). To examine whether regulation of neurite degeneration by ULK1 is autophagy dependent, we applied CHQ to block autophagy in control and *Ulk1* knockdown neurons. As expected, CHQ was able to suppress glutamate-induced neurite fragmentation in control neurons. However, CHQ treatment did not further inhibit neurite fragmentation in *Ulk1* knockdown neurons (*SI Appendix*, Fig. S8*C*). This suggests that ULK1 and CXQ are part of the same pathway and that the ability of ULK1 to regulate neurite degeneration is at least partly mediated through autophagy.

ULK1 Physically Interacts with SARM1. As ULK1 specifically colocalized with SARM1 in damaged axons after SCI, we examined the potential physical interaction between ULK1 and SARM1. In HEK293T cells transfected with exogenous HA-ULK1 and Myc-SARM1, immunoprecipitation (IP) of HA-ULK1 with either HA or ULK1 antibodies but not control immunoglobulin G (IgG) resulted in co-IP of Myc-SARM1 (Fig. 5 *A*–*C*). Similarly, IP of Myc-SARM1 resulted in co-IP of HA-ULK1 (Fig. 5 *D* and *E*). Both ULK1 (30) and SARM1 (6) have been reported to interact with TRAF6. However, the observed ULK1–SARM1 co-IP was independent of the transfection of exogenous FLAG-TRAF6 (Fig. 5 *A*–*E*). Therefore, either TRAF6 is not required or the endogenous levels of TRAF6 are sufficient for ULK1–SARM1 complex formation. These data suggest that the effects of autophagy on axonal degeneration could be mediated by physical interaction between ULK1 and SARM1.

In addition to the TIR domain mediating its NADase function, SARM1 protein includes autoinhibitory ARM domain and SAM domains important for oligomerization (*SI Appendix*, Fig. S9). To further characterize the interaction between ULK1 and SARM1, we created a series of *Sarm1* deletion mutants. Deletion of either ARM or TIR domains did not affect the ability of Myc-SARM1 to interact with HA-ULK1. However, deletion of the SAM region largely prevented the interaction, suggesting that the SAM domains participate in ULK1–SARM1 complex formation (Fig. 5*F* and *SI Appendix*, Fig. S9).

We investigated the interaction between endogenous ULK1 and SARM1 in primary cortical neurons. IP with antibody against either ULK1 or SARM1 but not the control IgG was able to bring down the ULK1–SARM1–containing complex (Fig. 5*G*). The interaction between endogenous SARM1 and ULK1 was increased in neurons after 1-h glutamate treatment (Fig. 5*H*). These data demonstrate that the physical interaction between endogenous ULK1 and SARM1 is related to glutamate excitotoxicity in neurons. Glutamate treatment also significantly increased the S555 phosphorylation of ULK1, consistent with its activation. ULK1 kinase inhibitor SBI significantly reduced phosphorylation of ULK1 (Fig. 5 *G*, *Left* [input] and *I*) and attenuated levels of ATG13pS318 in glutamate-treated neurons (*SI Appendix*, Fig. S7*D*). However, it did not significantly alter the extent of ULK1–SARM1 interaction (Fig. 5*H*). Together with data from Fig. 4 demonstrating the ability of SBI to attenuate the accumulation of SARM1 in neurites and the extent of glutamate-induced neurite fragmentation (Fig. 4 *B*, *D*, and *F* and *SI Appendix*, Fig. S8*A*), these data suggest that while ULK1 kinase activity may not be required for ULK1–SARM1 complex formation, it influences the ability of ULK1 to regulate SARM1 localization and function.

To investigate the ULK1–SARM1 interaction in vivo, we immunoprecipitated ULK1 from mouse sham and SCI spinal cord tissue. IP with antibodies against endogenous ULK1 was able to bring down SARM1 protein, demonstrating that ULK1–SARM1–containing complexes can form in the spinal cord tissue (Fig. 5*J*). The interaction was absent when control IgG was used.

Axonal Accumulation of ULK1 and SARM1 after SCI Is Attenuated in *Becn1*$^{+/-}$ Mice. To investigate the functional relevance of the interaction between ULK1 and SARM1 in vivo after SCI, we evaluated the expression and localization of SARM1 in *GFP-LC3* transgenic *Becn1*$^{+/-}$ autophagy hypomorph mice (31). One hour after SCI, SARM1 protein levels as well as phosphorylation of ULK1 significantly increased in wild-type (WT) microdissected dorsal column tissue, which contains CST and Gr tract axons but no neuronal cell bodies (Fig. 6*A*). *Becn1*$^{+/-}$ mice showed reduced phosphorylation of ULK1 in the dorsal column, confirming attenuated autophagy levels and ULK1 activation after SCI (Fig. 6*A*). Supporting involvement of ULK1 in the regulation of SARM1 during axonal degeneration, *Becn1*$^{+/-}$ mice also showed significant reduction in SARM1 accumulation in the dissected dorsal column tissue after SCI. Consistent with our in vitro data demonstrating that ULK1 affects SARM1 in neurites but not neuronal cell bodies, we did not observe significant differences in SARM1 levels between WT and *Becn1*$^{+/-}$ mice in the whole spinal cord, which contains both neuronal cell bodies and axons.

Using immunostaining, at 1 d after SCI, we observed a similar number of LC3^{+} swollen axonal bulbs in *Becn1*$^{+/-}$ mice compared to WT controls (*SI Appendix*, Fig. S10*A*). However, in *Becn1*$^{+/-}$ animals, the bulbs tended to have lower SARM1 intensity (*SI Appendix*, Fig. S10*B*). In the injured but nonswollen axons, LC3 significantly accumulated in WT mice but not *Becn1*$^{+/-}$ mice after SCI (Fig. 6*B*). Accumulation of both ULK1 and SARM1 in the injured axons was also decreased in the *Becn1*$^{+/-}$ mice compared to the WT mice (Fig. 6 *C* and *D*). We also observed a trend toward decrease in colocalization between ULK1 and SARM1, although this failed to reach statistical significance (*SI Appendix*, Fig. S10*C*). These data indicate that *Becn1*$^{+/-}$ mice are deficient in ULK1 and LC3 recruitment to the injured axons and that inhibition of axonal autophagy and ULK1 activity results in decreased SARM1 accumulation.

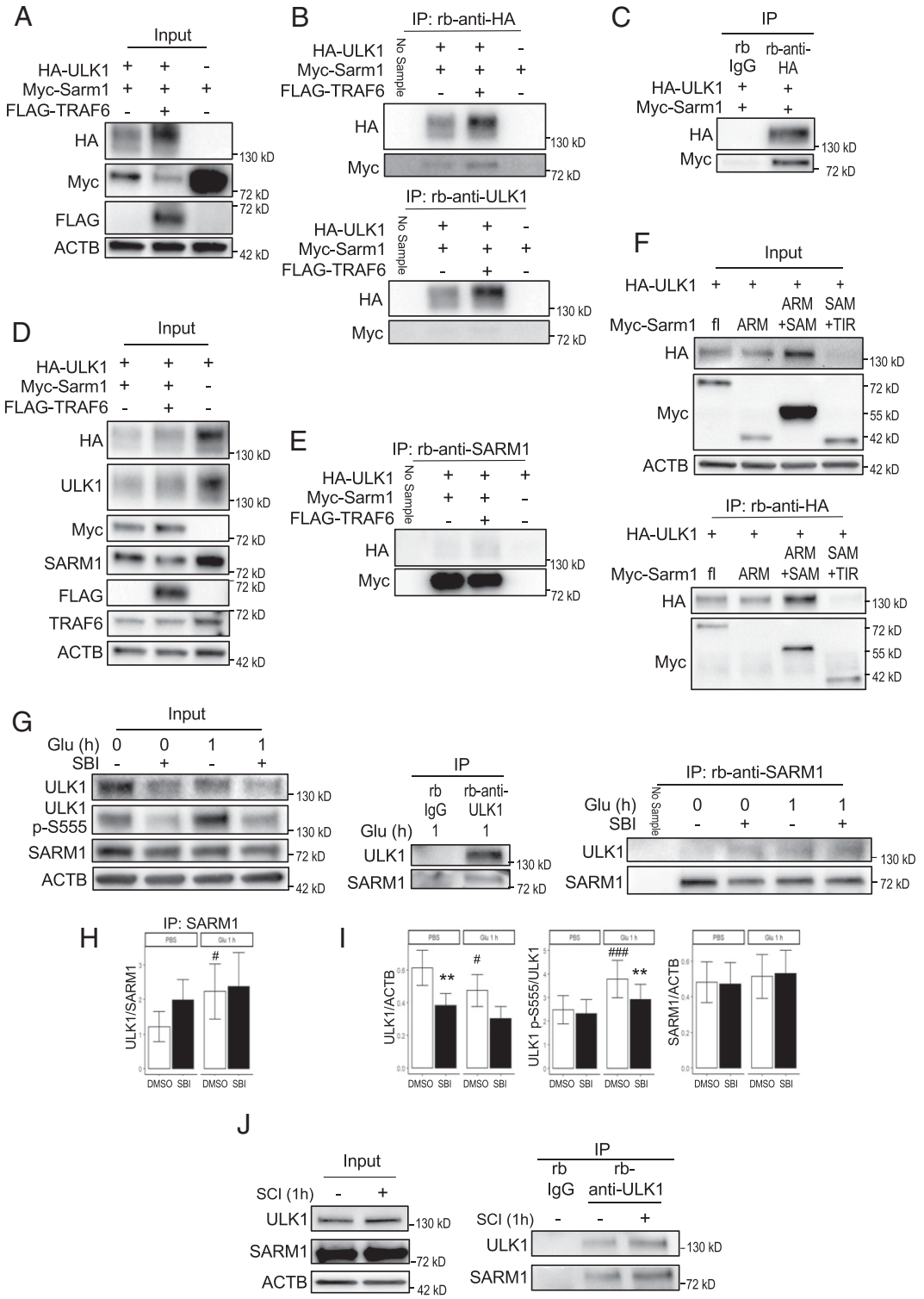

Fig. 5. ULK1 and SARM1 physically interact in vitro and in mouse spinal cord. (*A-E*) HA-ULK1, Myc-SARM1, and FLAG-TRAF6 were transfected into HEK293T cells as indicated. (*A-C*) ULK1 was immunoprecipitated using either HA or ULK1 antibodies. Myc-SARM1 was detected in the complexes immunoprecipitated from cells expressing HA-ULK1 but not from controls lacking HA-ULK1 or when control rabbit IgG was used, demonstrating physical interaction between ULK1 and SARM1. (*D* and *E*) SARM1 was immunoprecipitated using SARM1 antibodies. HA-ULK1 was detected in the complexes immunoprecipitated from cells expressing Myc-SARM1 but not from controls lacking Myc-SARM1, demonstrating physical interaction between ULK1 and SARM1. FLAG-TRAF6 did not cause obvious changes to the ULK1–SARM1 interaction in either experiment. (*F*) HEK293T cells were transfected with HA-ULK1 and either full-length (fl) Myc-SARM1 or indicated Myc-SARM1 truncation mutants. ULK1 was immunoprecipitated using antibody against HA; the presence of SARM1 in the complex was detected using Myc antibody. (*G*) Primary mouse cortical neurons were treated with glutamate (12.5 μM) in the presence of vehicle (dimethyl sulfoxide [DMSO]) or ULK1 inhibitor SBI (10 μM) for 1 h, followed by IP of endogenous ULK1 or SARM1. Rabbit IgG was used as control. (*H*) Quantification of SARM1 IP from *G*. Amount of ULK1 detected in SARM1 complexes increased significantly after 1-h glutamate (Glu) treatment but was not affected by SBI. #$P < 0.05$ versus no glutamate (phosphate-buffered saline [PBS]) controls treated with the same drug (DMSO or SBI). (*I*) Quantification of Western blot (input) data from *G*. Glutamate treatment significantly increased the phosphorylation of ULK1 at S555 while SBI significantly reduced ULK1 expression and phosphorylation. #$P < 0.05$, ###$P < 0.001$ versus no glutamate (PBS) controls treated with the same drug (DMSO or SBI). **$P < 0.01$ versus DMSO (vehicle) at the same time point (two-way ANOVA). At least three independent sets of experiments were included. Data are presented as mean ± SEM. (*J*) Endogenous ULK1 was immunoprecipitated from naive or SCI (1 h) mouse spinal cord tissue. SARM1 was detected in complexes with ULK1 but not in control IPs using rabbit IgG.

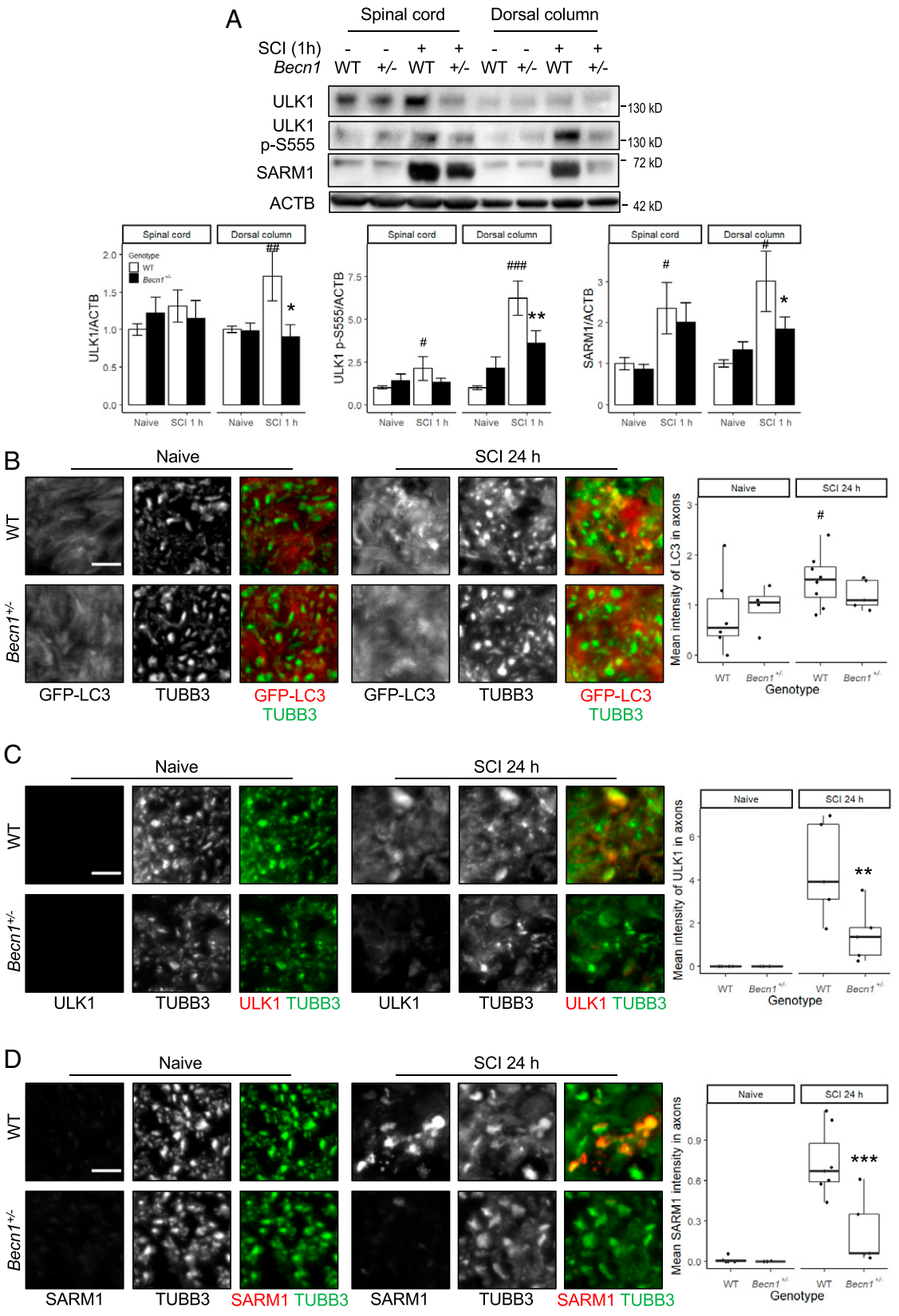

Fig. 6. *Becn1*$^{+/-}$ mice show attenuated activation of ULK1 and decreased SARM1 accumulation in injured axons after SCI. (*A*) SARM1 and ULK1 protein levels and ULK1 activation (S555 phosphorylation) in spinal cord segments around the injury site and in microdissected dorsal column tissue of WT and *Benc1*$^{+/-}$ mice 1 h after SCI. Total ULK1, p-S555 ULK1, and SARM1 levels increased in WT mice following injury, particularly in the dorsal column. All changes were attenuated in injured *Becn1*$^{+/-}$ mice. #$P < 0.05$, ##$P < 0.01$, ###$P<0.001$ versus naive of the same genotype; *$P < 0.05$, **$P < 0.01$ versus WT at the same time point (two-way ANOVA, $n = 5$ to 9). Data are presented as mean ± SEM. (*B*) GFP-LC3 levels in coronal spinal cord sections (RD area) from *GFP-LC3* (WT) and *Becn1*$^{+/-}$*;GFP-LC3* (*Becn1*$^{+/-}$) mice 24 h after SCI. GFP-LC3 accumulated in TUBB3^{+} injured axons of the RD area spinal cords from WT but not *Becn1*$^{+/-}$ mice. Scale bar, 10 μm. #$P < 0.05$ versus naive of the same genotype (two-way ANOVA, $n = 5$ to 8). (*C* and *D*) Attenuated accumulation of ULK1 (*C*) and SARM1 (*D*) in TUBB3^{+} axons of *Becn1*$^{+/-}$ mice compared to WT 24 h after SCI. Scale bar, 10 μm. **$P < 0.01$, ***$P < 0.001$ versus WT at the same time point (two-way ANOVA, $n = 5$ to 7). Each data point represents an individual mouse; boxplots show median and IQR measures.

Discussion

Previous studies demonstrated that autophagy and particularly the ULK1 kinase participate in mediation of axonal degeneration (12). However, the mechanisms of how autophagy may contribute to axonal degeneration are not fully understood. Recent studies suggest that autophagy may be required to provide energy for the active processes of axonal degeneration (10). ULK1 activation after neurotrauma was also demonstrated to promote axonal degeneration by regulating messenger RNA splicing and translation through the mTOR pathway (12). These mechanisms suggest that autophagy is necessary to provide metabolic and proteomic conditions favoring axonal degeneration. Our data demonstrate that the ULK1 kinase can also physically interact with and regulate the TIR NADase SARM1 required for mediation of axonal degeneration, suggesting an additional and more direct link between autophagy and the axonal degeneration machinery.

Despite recent progress, the mechanisms of how SARM1 is regulated in the context of axonal degeneration are not fully understood. Structural data demonstrate that SARM1 oligomerizes to form multimeric complexes bound to either oxidized nicotinamide-adenine dinucleotide (NAD^+; when inactive) or its precursor nicotinamide mononucleotide (NMN; when active) (32, 33). While replacement of NAD^+ with NMN is necessary for SARM1 activation, it is not sufficient for full activity. Phosphorylation, conformational changes, and transportation/translocation have all been suggested to participate in SARM1 activation (4, 32, 34–37). Our data demonstrating colocalization between activated ULK1 and SARM1 in axons within 1 h after SCI suggest that ULK1–SARM1 interaction may be one of the early events involved in the regulation of SARM1. Since pharmacological inhibition of ULK1 kinase or *Ulk1* knockdown in vitro as well as reduced ULK1 activity in *Becn1*$^{+/-}$ mice after SCI in vivo were associated with reduced accumulation of SARM1 only in neurites, but not in the neuronal cell bodies, we expect that ULK1 may specifically affect translocation of SARM1 from cell body to neurites. These data also indicate that ULK1 kinase activity is required for its effects on SARM1 localization. However, further studies will be necessary to define the biochemical mechanisms of how ULK1 may participate in the regulation of SARM1.

While ULK1 is primarily known for its role in the regulation of autophagy, more recently it has been shown to also play autophagy-independent functions, including in the regulation of intracellular trafficking, stress granule dynamics, and axonal pathfinding (29, 38–40). Therefore, it will be important to ascertain whether ULK1 function in the regulation of SARM1 during axonal degeneration is dependent or independent of autophagy. The ability of not only ULK1 but also the class III PI3 kinase and lysosomal inhibition to attenuate neurite degeneration and the accumulation of SARM1 in neurites supports the involvement of an autophagy-dependent pathway. The inability of autophagy inhibition by CHQ to provide further protection against neurite degeneration in *Ulk1* knockdown neurons also suggests that, in this context, ULK1 and autophagy are part of the same pathway. In vivo, ULK1 and SARM1 colocalized in injured axons and axonal bulbs with other autophagy proteins including LC3 and phospho-ATG13, supporting activation of autophagy. Furthermore, attenuation of both ULK1 activation and SARM1 accumulation was observed in dorsal column axons of *Becn1*$^{+/-}$ mice following SCI. These data are consistent with the role of ULK1 in the regulation of SARM1 and axonal degeneration being at least in part dependent on autophagy. One possibility is that ULK1 could recruit autophagy machinery to the SARM1 complex, providing the local energy required for its translocation to neurites. A similar role for autophagy as a local energy source has been suggested as necessary to promote exposure of phosphatidylserine as a phagocytic signal on the plasma membrane of transected axons (10).

Our data do not exclude the possibility of additional autophagy-independent function of ULK1 in the regulation of SARM1 during axonal degeneration, as has been observed in neurodevelopment (38). Since kinase activity of ULK1 is required, one possibility is that ULK1 could be involved in SARM1 phosphorylation, as has been previously reported for other nonautophagy-related proteins (38, 40). Another possibility is that the interaction between ULK1 and SARM1 could promote either stability of SARM1 in neurites or translocation of the complex to intracellular membranes such as the mitochondria (6). Alternatively, the proteins themselves may become less soluble after activation and/or interaction, as it has been suggested that the ULK1–ATG13 complex undergoes liquid-liquid phase separation upon activation (41). Future mechanistic studies, including comparisons between *Becn1*- and *Ulk1*-deficient cells and mice, will be necessary to further define the relationships between autophagy, ULK1, and SARM1 activity during axonal degeneration.

Dysregulation of autophagy and axonal degeneration are both implicated in neurotrauma and neurodegenerative diseases (42–45). However, the relationship between these pathways is complicated because autophagy appears to play a dual role in the injured neurons (46, 47). The present study as well as previous work focusing on axonal degeneration demonstrate that autophagy promotes acute neurite degeneration (10, 11, 48). On the other hand, autophagic flux is required for neuronal survival under both homeostatic and stress conditions by eliminating toxic protein aggregates and dysfunctional organelles (44, 45, 49, 50). We previously demonstrated that autophagy is impaired after neurotrauma including both SCI and traumatic brain injury (51–54). In rodent SCI models, inhibition of autophagy was specifically observed in the cell bodies of motor neurons in the ventral horn and contributed to both apoptotic and necroptotic cell death (52, 53). Consistent with the dual role of autophagy, our present study demonstrated that *Becn1*$^{+/-}$ autophagy hypomorph mice accumulated lower levels of axonal SARM1 than WT mice after SCI, indicating attenuation of axonal degeneration. However, in a separate study we recently demonstrated that these mice display exacerbated neuroinflammation, increased neuronal cell death, and worse functional outcomes at subacute and chronic time points after SCI (55). Together, these data confirm that the role of autophagy in axonal degeneration is spatiotemporally, functionally, and mechanistically distinct from its protective role in cell bodies (10–12, 52, 53).

Enhancement of autophagy has been proposed as a neuroprotective treatment in both neurotrauma and neurodegenerative diseases. However, the dual role of autophagy in promoting axonal degeneration and protection of neurons against cell death uncovered in the present and several other recent studies suggests that further investigations are warranted. Our data demonstrating direct interaction between ULK1 and SARM1 suggest that it may be possible to uncouple these functions by targeting different ULK1-containing complexes to differentially manipulate protective autophagy in cell bodies and SARM1 activation in neurites. However, further studies will be needed to confirm and identify the biochemical mechanisms and functional consequences of ULK1–SARM1 interaction in axonal degeneration.

Materials and Methods

Further experimental details are provided in the *SI Appendix*.

Contusive SCI Mouse Model. C57BL/6J young adult mice (9 to 11 wk, 20 to 25 g), *GFP-LC3* (56), *CX3CR1-GFP* (57), *Becn1*$^{+/-}$ (31), and *GFP-LC3*;*Becn1*$^{+/-}$ mice generated by crossing *GFP-LC3* and *Becn1*$^{+/-}$ were used. Following isoflurane anesthesia, laminectomy was performed. Mice underwent a moderate midline contusion injury at T10 level of the spinal cord with the Infinite Horizon Spinal Cord Impactor (Precision Systems and Instrumentation) with a force of 60 kilodyne (58, 59). All procedures were performed according to protocols approved by the University of Maryland School of Medicine Institutional Animal Care and Use Committee.

Statistical Analyses. All statistics were performed by RStudio. Boxplots show individual data points, median, and interquartile range (IQR) measures. Bar plots show mean ± SEM. In vivo sample sizes were estimated based on prior similar studies and pilot data. Multiway ANOVA and post hoc Dunnett comparison with Bonferroni correction were used. All tests were two-sided. The significance level was set at 0.05.

Data, Materials, and Software Availability. All study data are included in the article and/or *SI Appendix*.

ACKNOWLEDGMENTS. We thank the Electron Microscopy Core Imaging Facility for the access and technical support of correlative EM, Prof. Winnok H. De Vos, PhD, at Antwerp University for the provision and technical support of MorphoNeuroNet script, Dr. Boris Sabirzhanov for useful discussion, and Ms. Sabrina Bustos for mouse colony management. Research was supported by Grant Nos. R01NS094527 to J.W. and M.M.L.; R01NS091218 and R01NS115876 to M.M.L.; and R01NS110635, RF1NS110637, and R01NS110825 to J.W.

1. M. D. Figley, A. DiAntonio, The SARM1 axon degeneration pathway: Control of the NAD$^+$ metabolome regulates axon survival in health and disease. *Curr. Opin. Neurobiol.* **63**, 59–66 (2020).
2. J. Gerdts, D. W. Summers, J. Milbrandt, A. DiAntonio, Axon self-destruction: New links among SARM1, MAPKs, and NAD$^+$ metabolism. *Neuron* **89**, 449–460 (2016).
3. L. Conforti, J. Gilley, M. P. Coleman, Wallerian degeneration: An emerging axon death pathway linking injury and disease. *Nat. Rev. Neurosci.* **15**, 394–409 (2014).
4. P. Mukherjee *et al.*, SARM1, not MyD88, mediates TLR7/TLR9-induced apoptosis in neurons. *J. Immunol.* **195**, 4913–4921 (2015).
5. S. A. Killackey *et al.*, The mitochondrial Nod-like receptor NLRX1 modifies apoptosis through SARM1. *Mol. Cell. Biochem.* **453**, 187–196 (2019).
6. H. Murata, M. Sakaguchi, K. Kataoka, N. H. Huh, SARM1 and TRAF6 bind to and stabilize PINK1 on depolarized mitochondria. *Mol. Biol. Cell* **24**, 2772–2784 (2013).
7. E. Turkiew, D. Falconer, N. Reed, A. Höke, Deletion of Sarm1 gene is neuroprotective in two models of peripheral neuropathy. *J. Peripher. Nerv. Syst.* **22**, 162–171 (2017).
8. D. V. Bradshaw Jr. *et al.*, Genetic inactivation of SARM1 axon degeneration pathway improves outcome trajectory after experimental traumatic brain injury based on pathological, radiological, and functional measures. *Acta Neuropathol. Commun.* **9**, 89 (2021).
9. R. C. Russell *et al.*, ULK1 induces autophagy by phosphorylating Beclin-1 and activating VPS34 lipid kinase. *Nat. Cell Biol.* **15**, 741–750 (2013).
10. S. Wakatsuki, S. Tokunaga, M. Shibata, T. Araki, GSK3B-mediated phosphorylation of MCL1 regulates axonal autophagy to promote Wallerian degeneration. *J. Cell Biol.* **216**, 477–493 (2017).
11. J. Knöferle *et al.*, Mechanisms of acute axonal degeneration in the optic nerve in vivo. *Proc. Natl. Acad. Sci. U.S.A.* **107**, 6064–6069 (2010).
12. B. F. Vahsen *et al.*, Inhibition of the autophagic protein ULK1 attenuates axonal degeneration in vitro and in vivo, enhances translation, and modulates splicing. *Cell Death Differ.* **27**, 2810–2827 (2020).
13. N. Mizushima, A. Kuma, Autophagosomes in GFP-LC3 transgenic mice. *Methods Mol. Biol.* **445**, 119–124 (2008).
14. D. J. Klionsky *et al.*, Guidelines for the use and interpretation of assays for monitoring autophagy (4th edition). *Autophagy* **17**, 1–382 (2021).
15. V. T. Ribas *et al.*, Early and sustained activation of autophagy in degenerating axons after spinal cord injury. *Brain Pathol.* **25**, 157–170 (2015).
16. J. H. Joo *et al.*, Hsp90-Cdc37 chaperone complex regulates Ulk1- and Atg13-mediated mitophagy. *Mol. Cell* **43**, 572–585 (2011).
17. J. Gilley, R. R. Ribchester, M. P. Coleman, Sarm1 deletion, but not Wld^S, confers lifelong rescue in a mouse model of severe axonopathy. *Cell Rep.* **21**, 10–16 (2017).
18. M. J. Geden, M. Deshmukh, Axon degeneration: Context defines distinct pathways. *Curr. Opin. Neurobiol.* **39**, 108–115 (2016).
19. J. Vérièpe, L. Fossouo, J. A. Parker, Neurodegeneration in *C. elegans* models of ALS requires TIR-1/Sarm1 immune pathway activation in neurons. *Nat. Commun.* **6**, 7319 (2015).
20. T. Itoh *et al.*, ZPK/DLK and MKK4 form the critical gateway to axotomy-induced motoneuron death in neonates. *J. Neurosci.* **34**, 10729–10742 (2014).
21. E. Asghari Adib, L. J. Smithson, C. A. Collins, An axonal stress response pathway: Degenerative and regenerative signaling by DLK. *Curr. Opin. Neurobiol.* **53**, 110–119 (2018).
22. S. Karney-Grobe, A. Russo, E. Frey, J. Milbrandt, A. DiAntonio, HSP90 is a chaperone for DLK and is required for axon injury signaling. *Proc. Natl. Acad. Sci. U.S.A.* **115**, E9899–E9908 (2018).
23. C. D. Pozniak *et al.*, Dual leucine zipper kinase is required for excitotoxicity-induced neuronal degeneration. *J. Exp. Med.* **210**, 2553–2567 (2013).
24. D. W. Summers, J. Milbrandt, A. DiAntonio, Palmitoylation enables MAPK-dependent proteostasis of axon survival factors. *Proc. Natl. Acad. Sci. U.S.A.* **115**, E8746–E8754 (2018).
25. B. Grill, R. K. Murphey, M. A. Borgen, The PHR proteins: Intracellular signaling hubs in neuronal development and axon degeneration. *Neural Dev.* **11**, 8 (2016).
26. E. Babetto, B. Beirowski, E. V. Russler, J. Milbrandt, A. DiAntonio, The Phr1 ubiquitin ligase promotes injury-induced axon self-destruction. *Cell Rep.* **3**, 1422–1429 (2013).
27. E. Park, A. A. Velumian, M. G. Fehlings, The role of excitotoxicity in secondary mechanisms of spinal cord injury: A review with an emphasis on the implications for white matter degeneration. *J. Neurotrauma* **21**, 754–774 (2004).
28. D. E. Hernández *et al.*, Axonal degeneration induced by glutamate excitotoxicity is mediated by necroptosis. *J. Cell Sci.* **131**, jcs214684 (2018).
29. B. Wang, M. Kundu, Canonical and noncanonical functions of ULK/Atg1. *Curr. Opin. Cell Biol.* **45**, 47–54 (2017).
30. F. Nazio *et al.*, mTOR inhibits autophagy by controlling ULK1 ubiquitylation, self-association and function through AMBRA1 and TRAF6. *Nat. Cell Biol.* **15**, 406–416 (2013).
31. X. Qu *et al.*, Promotion of tumorigenesis by heterozygous disruption of the beclin 1 autophagy gene. *J. Clin. Invest.* **112**, 1809–1820 (2003).
32. M. Bratkowski *et al.*, Structural and mechanistic regulation of the pro-degenerative NAD hydrolase SARM1. *Cell Rep.* **32**, 107999 (2020).
33. S. Sambashivan, M. R. Freeman, SARM1 signaling mechanisms in the injured nervous system. *Curr. Opin. Neurobiol.* **69**, 247–255 (2021).
34. H. Murata *et al.*, c-Jun N-terminal kinase (JNK)-mediated phosphorylation of SARM1 regulates NAD$^+$ cleavage activity to inhibit mitochondrial respiration. *J. Biol. Chem.* **293**, 18933–18943 (2018).
35. J. Gerdts, D. W. Summers, Y. Sasaki, A. DiAntonio, J. Milbrandt, Sarm1-mediated axon degeneration requires both SAM and TIR interactions. *J. Neurosci.* **33**, 13569–13580 (2013).
36. D. W. Summers, D. A. Gibson, A. DiAntonio, J. Milbrandt, SARM1-specific motifs in the TIR domain enable NAD$^+$ loss and regulate injury-induced SARM1 activation. *Proc. Natl. Acad. Sci. U.S.A.* **113**, E6271–E6280 (2016).
37. J. Gerdts, E. J. Brace, Y. Sasaki, A. DiAntonio, J. Milbrandt, SARM1 activation triggers axon degeneration locally via NAD+ destruction. *Science* **348**, 453–457 (2015).
38. B. Wang *et al.*, The autophagy-inducing kinases, ULK1 and ULK2, regulate axon guidance in the developing mouse forebrain via a noncanonical pathway. *Autophagy* **14**, 796–811 (2018).
39. B. Wang *et al.*, ULK1 and ULK2 regulate stress granule disassembly through phosphorylation and activation of VCP/p97. *Mol. Cell* **74**, 742–757.e8 (2019).
40. J. H. Joo *et al.*, The noncanonical role of ULK/ATG1 in ER-to-Golgi trafficking is essential for cellular homeostasis. *Mol. Cell* **62**, 491–506 (2016).
41. N. N. Noda, Z. Wang, H. Zhang, Liquid-liquid phase separation in autophagy. *J. Cell Biol.* **219**, e202004062 (2020).
42. R. Adalbert, M. P. Coleman, Review: Axon pathology in age-related neurodegenerative disorders. *Neuropathol. Appl. Neurobiol.* **39**, 90–108 (2013).
43. N. Salvadores, M. Sanhueza, P. Manque, F. A. Court, Axonal degeneration during aging and its functional role in neurodegenerative disorders. *Front. Neurosci.* **11**, 451 (2017).
44. F. M. Menzies, A. Fleming, D. C. Rubinsztein, Compromised autophagy and neurodegenerative diseases. *Nat. Rev. Neurosci.* **16**, 345–357 (2015).
45. H. Park, J.-H. Kang, S. Lee, Autophagy in neurodegenerative diseases: A hunter for aggregates. *Int. J. Mol. Sci.* **21**, 3369 (2020).
46. Y. Wang, M. Song, F. Song, Neuronal autophagy and axon degeneration. *Cell. Mol. Life Sci.* **75**, 2389–2406 (2018).
47. Y. Yang, M. Coleman, L. Zhang, X. Zheng, Z. Yue, Autophagy in axonal and dendritic degeneration. *Trends Neurosci.* **36**, 418–428 (2013).
48. Q. J. Wang *et al.*, Induction of autophagy in axonal dystrophy and degeneration. *J. Neurosci.* **26**, 8057–8068 (2006).
49. T. E. Moors *et al.*, Therapeutic potential of autophagy-enhancing agents in Parkinson's disease. *Mol. Neurodegener.* **12**, 11 (2017).
50. F. M. Menzies *et al.*, Autophagy and neurodegeneration: Pathogenic mechanisms and therapeutic opportunities. *Neuron* **93**, 1015–1034 (2017).
51. C. Sarkar *et al.*, Impaired autophagy flux is associated with neuronal cell death after traumatic brain injury. *Autophagy* **10**, 2208–2222 (2014).
52. S. Liu *et al.*, Disrupted autophagy after spinal cord injury is associated with ER stress and neuronal cell death. *Cell Death Dis.* **6**, e1582 (2015).
53. S. Liu *et al.*, Lysosomal damage after spinal cord injury causes accumulation of RIPK1 and RIPK3 proteins and potentiation of necroptosis. *Cell Death Dis.* **9**, 476 (2018).
54. Y. Li *et al.*, cPLA2 activation contributes to lysosomal defects leading to impairment of autophagy after spinal cord injury. *Cell Death Dis.* **10**, 531 (2019).
55. Y. Li *et al.*, Impairment of autophagy after spinal cord injury potentiates neuroinflammation and motor function deficit in mice. *Theranostics* **12**, 5364–5388 (2022).
56. N. Mizushima, A. Yamamoto, M. Matsui, T. Yoshimori, Y. Ohsumi, In vivo analysis of autophagy in response to nutrient starvation using transgenic mice expressing a fluorescent autophagosome marker. *Mol. Biol. Cell* **15**, 1101–1111 (2004).
57. S. Jung *et al.*, Analysis of fractalkine receptor CX(3)CR1 function by targeted deletion and green fluorescent protein reporter gene insertion. *Mol. Cell. Biol.* **20**, 4106–4114 (2000).
58. J. J. Matyas *et al.*, Truncated TrkB.T1-mediated astrocyte dysfunction contributes to impaired motor function and neuropathic pain after spinal cord injury. *J. Neurosci.* **37**, 3956–3971 (2017).
59. J. Wu *et al.*, Endoplasmic reticulum stress and disrupted neurogenesis in the brain are associated with cognitive impairment and depressive-like behavior after spinal cord injury. *J. Neurotrauma* **33**, 1919–1935 (2016).